Impact of Climate Change on River Flow Regimes in Japanese Catchments using GCM Hydrologic Projections and a Distributed Rainfall-Runoff Model

Yasuto TACHIKAWA
Department of Urban and Environmental Engineering, Kyoto University, Kyoto 615-8540, Japan

1 INTRODUCTION

Global warming will give us a serious impact on our life. Frequencies and magnitudes of floods and sedimentation disasters are predicted to increase due to the change of precipitation extremes. Storm surges and inundation disasters at the coastal and low-land areas are likely to increase due to sea level rise and the changes of typhoon magnitudes. The IPCC, the Intergovernmental Panel on Climate Change, 4th assessment report published in 2007 describes increase of global average surface temperatures, increase of global average sea level, potential increase of frequency of heavy rainfall, and so on based on long term observations. The report also shows the projections of climate change according to several greenhouse gas emission scenarios and the impacts of climate change on water-related disasters and water resources.

To cope with water-related disasters induced by climate change, both mitigation measures and adaptation measures are essential. Mitigation measures are efforts to reduce greenhouse gases, and adaptation measures are actions to avoid/mitigate disasters under global warming. Research institutes specializing disaster prevention/mitigation and governmental organizations have responsibility to predict future climate and possible water-related disasters, and to make planning and implementation for adaptation measures. To establish adaptation measures, the following are quite important themes to be studied together across the related fields:

1) Projection of the future extremes, especially precipitation and typhoon developments, using advanced atmospheric models.
2) Impact analyses of climate change on water-related disasters. Analyses of the changes in frequency and magnitude of water-related disasters such as floods, sedimentations, storm surges, inundations and droughts using future climate projection data are essential to establish adaptation maesures.
3) Planning and implementation of adaptation measures based on the impact analysis studies of climate change on water-related disasters.

Projection of future climate is the area of climate and meteorology researchers and its related institutes. In Japan, MRI (Meteorological Research Institute, Japan Meteorology Agency) and CCSR (Center for Climate System Research, the University of Tokyo) develop their own GCMs (General Circulation Models), and provide future climate projections under a greenhouse gases scenario. Impact analyses of climate change on water-related disasters are the research fields of hydrology, water resources engineering, river engineering, and coastal engineering.

To effectively promote the research for better projection under climate change and its potential impact on natural disasters, MEXT, the Ministry of Education, Culture, Sports Science and Technology Japan, launched a 5-year (FY2007-02011) initiative called the Innovative Program of Climate Change Projection for the 21st Century (KAKUSHIN Program). In the KAKUSHIN Program, MRI and CCSR have a mission to enhance prediction abilities of their GCMs and provide projection data to the research communities. Disaster Prevention Research Institute and Engineering Department at Kyoto University etc. have responsibility for the impact studies on water-related disasters, which will contribute to the planning and implementation of adaptation measures.

In the KAKUSIN Program, DPRI and Engineering Department of Kyoto University have organized the research project entitled “Integrated assessment of climate change impacts on watersheds in a disaster environment (PI: Prof. Eiichi Nakakita)”, making up a team with MRI to contribute disaster environment assessment research. The research topics include the following:

- Rainfall extremes: Integrated analysis of rainfall extremes for Japan and over the globe in various time and space scales; Development of statistical and physical down scaling methods to obtain regional scale precipitation.
- Floods and water resources: Development of distributed hydrologic models and application to major Japanese catchments to assess the impact of climate change on flood and drought risk; Development

of integrated dam operation strategies to cope with floods and draughts by fully utilizing the existing structures.

- Inundations: Analysis of potential changes of inundation disasters in frequency and magnitude at Japanese major cities such as Tokyo, Nagoya, Kyoto, Osaka and Fukuoka.
- Sedimentations: Analysis of potential changes of sedimentation disasters in frequency and magnitude at various Japanese mountainous catchments.
- Strom surges: Risk assessment of storm surges and tidal waves at Tokyo Bay, Ise Bay, and Osaka Bay using a stochastic typhoon model; Reliability analysis of bank protection for extreme typhoons simulated by a regional climate model.
- Strong winds: Development of a strong wind disaster assessment model which predicts the damage ratio of buildings and structures; Estimation of the damage ratios at local authority level over Japan for possible typhoons under climate change.

In this presentation, floods and water resources are focused, and the recent research results of possible changes of river discharge regimes under climate change are presented. In section 2, a basic knowledge of the kinematic wave theory for rainfall-runoff simulation is presented. In section 3, a high resolution distributed hydrologic model to assess future hydrologic change in catchment scale is described. Then, in section 4, the lumping method of the distributed hydrologic model to reduce the computational burden is presented. In section 5, the hydrologic model ODIS-LEM (OHyMoS based distributed hydrologic model with lumped element models) is applied to the Mogami River basin (7,040km^2) and the Yoshino River basin (3,750km^2) in Japan for river discharge simulations using high resolution climate change projections with 20km and 1hr space and time resolution for current climate (1979 to 2004), near future (2015 to 2039) and future climate (2075-2099) developed by MRI in Japan. The hydrologic model ODIS-LEM simulates water flows based on Digital Elevation Models, channel networks and land use, which enables long term hydrologic simulations with hourly time resolution to assess the change of water resources and extreme events in catchment scale.

The Mogami River basin is a typical catchment with heavy snowfall in winter season and the snow melting is important water resources for rice planting in spring. The Yoshino River basin is located at the south part of Japan having heavy rainfall caused by rainy front and typhoons in summer season. It is revealed at the Mogami River basin that the differences of annual and monthly precipitations between present-day and future climate are small; but the differences of annual and monthly snowfall between present-day and future climate is quite large and snowfall in future climate decreases drastically. The simulated river discharge show that monthly peak discharge which happens from March to May in the present climate shifts to January to March in the future climate; and river discharge in April and May in the future climate much decreases. At the Yoshino River basin, the magnitude and frequency of severe rainfall would increase and peak flood discharge would increase more highly in the future climate (Tachikawa *et al.*, 2009).

2 KINEMATIC WAVE MODEL

The kinematic wave model was originally developed for river routing, then, it was applied to catchment rainfall-runoff modeling. Several variations of the kinematic wave model were developed to improve the prediction accuracy of rainfall-runoff from catchments. These models realize various flow mechanisms, characteristics of soil and land use, and these spatial distributions within a catchment.

2.1 Basic theory

The basic form of the kinematic wave equation is

$$\frac{\partial A}{\partial t} + \frac{\partial Q}{\partial x} = q_L(x,t) \tag{1}$$

$$Q = \alpha A^m \tag{2}$$

where $A(x, t)$ is the flow cross-sectional area, $Q(x, t)$ is the flow discharge, $q_L(x, t)$ is the lateral inflow discharge per unit length, and α and m are constants.

Equation (1) is the continuity equation and is derived from the principle of mass conservation within a control volume. Equation (2) is derived from Manning's or Chezy's laws, which are flow resistance laws of open channel uniform flow. Manning's law is described as:

$$v = \frac{1}{n} I^{1/2} R^{2/3} \tag{3}$$

in which v is the average flow velocity, n is Manning's friction coefficient, R is the hydraulic radius, and I is the friction slope. By assuming that R can be generally expressed as $z_1 A^{z_2}$ (z_1 and z_2 are constants), we can easily obtain the expression of Equation (2).

2.2 Kinematic wave model for shallow surface water flow on a rectangular plane

A catchment is often modeled as a rectangular plane or a set of rectangular planes, and rainfall-runoff from a catchment is modeled as shallow water flow on a rectangular plane (or rectangular planes). The hydraulic radius of shallow water flow can be approximated by the water depth h. Then, Equation (3) is written as:

$$v = \frac{1}{n} I^{1/2} h^{2/3} \tag{4}$$

Therefore the discharge per unit width q is expressed as:

$$q = vh = \frac{1}{n} I^{1/2} h^{5/3} = \alpha h^m \tag{5}$$

in which $\alpha = \sqrt{I}/n$, m = 5/3. This equation is the kinematic wave equation for shallow water flow on a rectangular plane. By dividing both sides of Equation (1) by the width of a rectangular plane B, the continuity equation bocomes

$$\frac{\partial h}{\partial t} + \frac{\partial q}{\partial x} = r = q_L / B \tag{6}$$

where, r is rainfall intensity. The value of I is usually approximated as the slope gradient of the rectangular plane, and the value of n is calibrated from observation or determined empirically.

2.3 Kinematic wave model for surface-subsurface saturated flow (Takasao & Shiiba, 1988)

The kinematic wave model described above is applied to infiltration excess overland flow (Hortonian overland flow). To extend the discharge-depth relationship to represent saturation excess overland flow, Takasao and Shiiba (1988) developed a new discharge-depth relationship which includes both surface and subsurface flow and its interaction. They assumed that hillslope surface was covered by a soil layer with high surface infiltration capacity and permeability, which is illustrated in Figure 1. In this figure, D is the depth of the soil layer, L is the length of the hillslope, H is the depth of water flow, and r is the rainfall intensity. Let γ be the porosity of the soil layer and be spatially constant. Then the depth of the effective pore of the soil layer, d, becomes γD. Also, the actual water depth (water volume in height), h, becomes γH ($0 < H < D$) or $H\text{-}D\text{+}\gamma D$ ($H > D$). Takasao and Shiiba (1988) derived the following relation between h and q from Darcy's law and Manning's law:

$$q = \begin{cases} ah, & 0 \le h \le d \\ \alpha (h-d)^m + ah, & h \ge d \end{cases} \tag{7}$$

where $a = k \sin\theta / \gamma$ is the velocity of water which flows in the soil layer, k is the hydraulic conductivity, and $\alpha = \sqrt{\sin\theta}/n$ and m=5/3, respectively. The upper relation given in Equation (7) is used for the case where only

subsurface flow occurs, and the lower relation in Equation (7) is used for the case where saturation excess overland flow occurs.

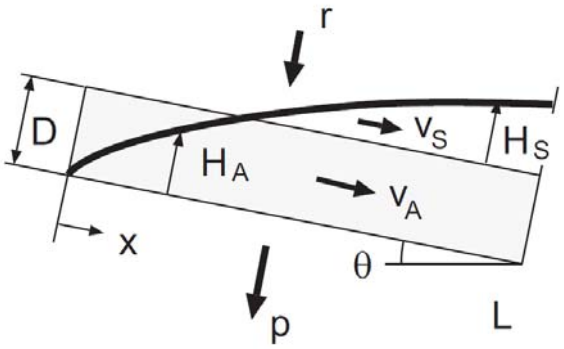

Figure 1. Schematic drawing of surface-subsurface flow on a hillslope.

2.4 Kinematic wave model for surface-subsurface saturated-unsaturated flow (Tachikawa et al., 2005)

The kinematic wave models described in 2.2 and 2.3 are basically used to simulate flood runoff which occurs in heavy rainfall events where the gravity force is dominant as a driving force of water flow. However these discharge-stage relations can not be used in drier conditions because the capillary force of soil particles can not be negligible in comparison with the gravity force in such conditions. To realize long term runoff simulations from dry to humid seasons continuously, Tachikawa *et al.* (2005) further extended the discharge-stage relation to realize both high flow and low flow simulation introducing an unsaturated flow mechanism in capillary pore of hillslope soil layer.

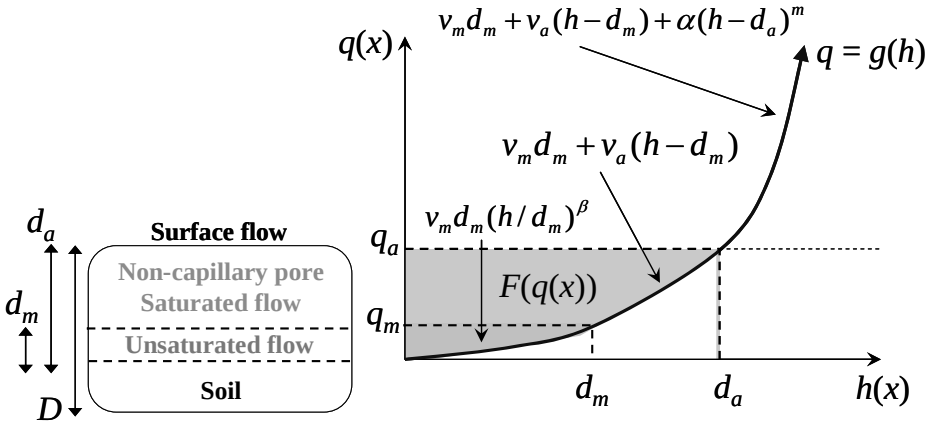

Figure 2. Schematic drawing of saturated-unsaturated flow and the *f*, *g*, and *F* relationships in section 4.

The discharge depth relation realizes three lateral flow mechanisms including 1) subsurface flow through capillary pore; 2) subsurface flow through non-capillary pore; and 3) surface flow on the soil layer. At a slope segment, when the water depth is lower than the equivalent water depth for unsaturated flow ($0 < h < d_m$), flow is simulated by Darcy law with an unsaturated hydraulic conductivity k_m. If the water depth exceeds the equivalent depth for unsaturated flow, the exceeded water flows as saturated subsurface flow that is simulated by Darcy law with saturated hydraulic conductivity k_a. Once the water depth is greater than the soil layer D times effective porosity γ ($d_a = \gamma D$), the water flows as surface flow, which is simulated by the Manning's equation. These three flow processes are represented by the following single set of stage-discharge relationship represented in Figure 2 and Equation 8) and the continuity equation (Tachikawa *et al.*, 2004; Sayama and McDonnel, 2009):

$$q = \begin{cases} v_m d_m (h/d_m)^{\beta}, & 0 \le h \le d_m \\ v_m d_m + v_a (h - d_m), & d_m \le h \le d_a \\ v_m d_m + v_a (h - d_m) + \alpha (h - d_a)^m, & d_a \le h \end{cases} \quad (8)$$

$$v_m = k_m i, \quad v_a = k_a i, \quad k_m = k_a / \beta, \quad \alpha = \sqrt{i}/n$$

$$c^* = \frac{\partial q}{\partial h} = \begin{cases} \beta v_m (h/d_m)^{\beta-1}, & 0 \le h \le d_m \\ v_a, & d_m \le h \le d_a \\ v_a + m\alpha (h - d_a)^{m-1}, & d_a \le h \end{cases} \quad (9)$$

where q is discharge per unit width, h is water depth, i is the slope gradient, k_m is the saturated hydraulic conductivity of the capillary soil layer, k_a is the hydraulic conductivity of the non-capillary soil layer, d_m is the depth of the capillary soil layer, d_a represents the depths of the capillary and non-capillary soil layers, β is the exponent constant of unsaturated flow, v_m and v_a are the flow velocities of unsaturated and saturated subsurface flows, respectively, and n is the Manning's roughness coefficient which varies as a function of land use type. Model parameters in the stage-discharge relationship are d_m, k_m, d_a, k_a, n, and β (= k_a/ k_m). The kinematic wave celerity for each layer is formulated in Equation 9.

3 DISTRIBUTED HYDROLOGIC MODEL WITH KINEMATIC WAVE THEORY

3.1 Open-book type catchment modeling and Kinematic wave flow

The simplest application of the kinematic wave model is to apply the model to an open-book catchment model. Figure 3 illustrates a schematic representation of an open-book catchment model. As its name implies, an open-book catchment model consists of two rectangular planes and a stream. Rain water flows on the planes and drains into the stream. The streamflow drains out of the catchment outlet. The flows on the rectangular planes and the stream are routed using the kinematic wave model. This is the simplest approximation of catchment hydrology using a kinematic wave model. A more complex structure of a catchment can be modeled as a cascade of the open-book catchment model.

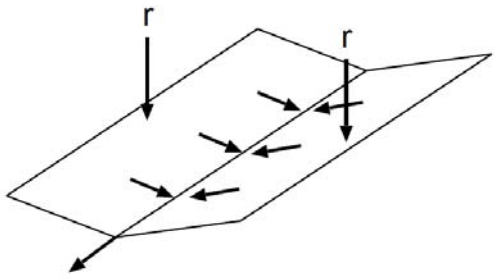

Figure 3. Schematic drawing of an open-book catchment modeling.

3.2 Catchment modeling using Digital Elevation Models and Kinematic wave flow

Digital elevation models are available at any catchments with a high resolution enough to describe the topography of catchments. Figure 4 is an example of a flow direction map derived from a grid-based DEM using the 8-direction method. After deriving the flow direction map, it is easy to define a rectangular plane formed by two adjacent grid points as shown in Figure 5. Catchment topography is represented by a set of slope units. For each slope unit, its area, length and gradient are easily calculated. The kinematic wave model is applied to all slope units and rainfall is routed according to the flow direction mapping. The outflow discharge from the catchment was used as the lateral inflow condition of a river routing model.

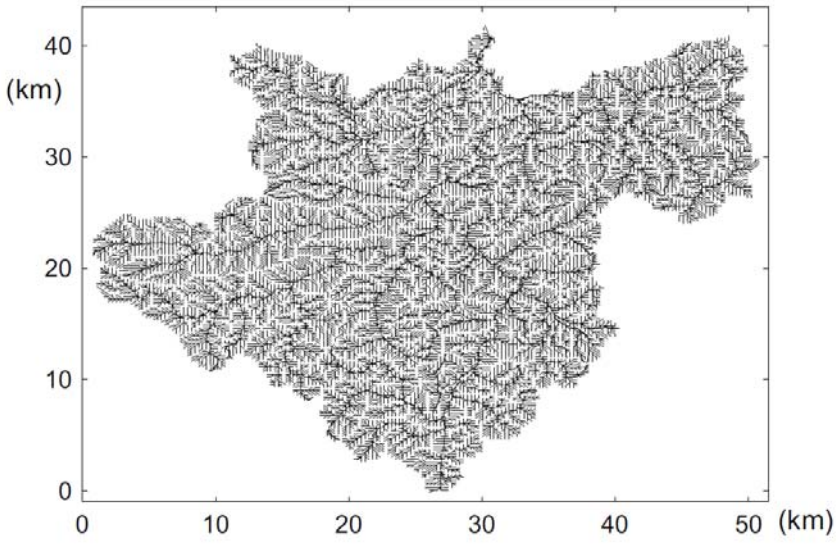

Figure 4. Flow direction mapping using DEM at the Maruyama Basin in Japan.

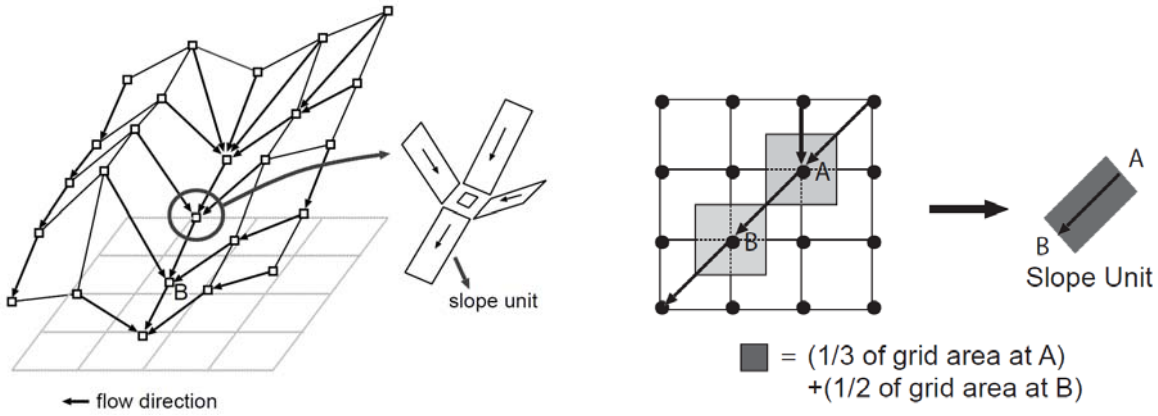

Figure 5. Schematic drawing of a catchment modelling using DEM. Left: Connection of slope unit. Right: Calculation of the area, length, gradient of a slope unit.

4 LUMPING OF DISTRIBUTED RAINFALL-RUNOFF MODELS

Distributed runoff models are based on physical hydrological processes. It is a strong point of distributed models; however they require much computational time and computer resources. For long time simulation such as discharge simulation under climate change, a lumping method of distributed models is essential to reduce the computational burden. In this section, a lumped kinematic wave runoff model is derived by spatially integrating the kinematic wave model described in 2.4. The derived lumped model has a physical basis and the parameter values are determined using topographic variables obtained from DEMs.

The lumping method is based on Ichikawa and Shiiba (2002). The fundamental assumption is that the rainfall-runoff process of the catchment system reaches a steady state with spatially uniform rainfall input. From this assumption, discharge from the catchment is expressed as a product of rainfall intensity and the upslope contributing area. Then, the relationship between the total amount of stored water in the catchment and the outflow discharge from the catchment is theoretically derived by integration of spatially distributed equations assigned to each sub-catchment over the entire catchment.

From the stage-discharge relationship in Equation (8), a general kinematic wave equation can be expressed as $q = g(h)$, and it is assumed q is possible to integrate with h. Furthermore, it is assumed h is explicitly expressed by q as the equation of $h = f(q)$. As shown in Figure 6, the discharge per unit width in each rectangular slope is given at the steady state assumption as:

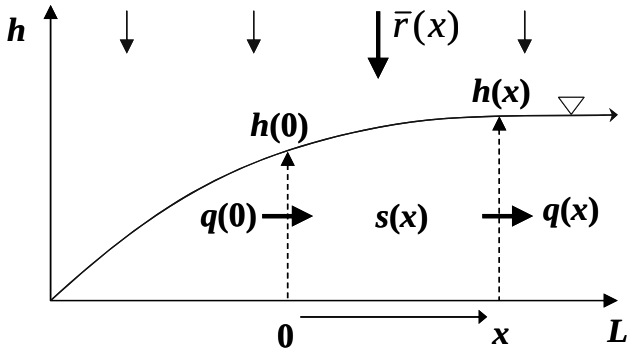

Figure 6. Relation between flow variables and storage in a slope unit.

$$q(x) = q(0)/w + \bar{r}\int_0^x (x)\ dx = \bar{r}\,U/w + \bar{r}\,x \tag{10}$$

where is $\bar{r}$ the rainfall intensity, U is the upslope contributing area, x is the horizontal distance (slope length) from the upstream end of a slope unit, and w is the width of the slope unit. According to Figure 6, the stored water volume of a slope unit, s, is given as a function of cross-sectional area A, which can be derived by the integration of h from 0 to x as follows:

$$s = \int_0^x A(x)\,dx = w\int_0^x h(x)\,dx \tag{11}$$

By substituting the variable of integration from x to q using the relationship given by Equation (10), $dq = r\,dx$, and the relationships $h = f(q)$ and $q = g(h)$, then Equation (11) becomes

$$s = \frac{w}{\bar{r}}\int_{q(0)}^{q(x)} f(q)\ dq = \frac{w}{\bar{r}}\left[F(q(x)) - F(q(0))\right] \tag{12}$$

As mentioned above, h is assumed to be a function of q. However, f cannot always be solved explicitly since q is also a function of h. In this case, F cannot be analytically quantified. Figure 2 schematically displays the relationships between f, g, and F. This figure assumes that g is a function of h and that it can be analytically integrated with h; the figure gives a solution for how to obtain F.

According to Figure 2, if the value of q is known from Equation (10), and h is numerically obtained using Equation (8), then $F(q(x))$ can be calculated. The equation s to obtain the value of $F(q(x))$ is as follows:

For an unsaturated flow condition ($q(x)$ less than or equal to q_m), $q_m = V_m d_m$:

$$F(q(x)) = q(x)h(x) - \int_0^{h(x)} g(h)dh = q(x)h(x) - \int_0^{h(x)} V_m d_m \left(\frac{h}{d_m}\right)^{\beta} dh$$

and it is reduced to

$$F(q(x)) = q(x)h(x) - \frac{V_m h^{\beta+1}}{\beta+1\, d_m{}^{\beta-1}} \tag{13}$$

For a saturated flow condition ($q(x)$ less than or equal to q_a), $q_a = V_m d_m + V_a(d_a - d_m)$:

$$F(q(x)) = q(x)h(x) - \int_0^{d_m} V_m d_m \left(\frac{h}{d_m}\right)^{\beta} dh - \int_{d_m}^{h(x)} \left(V_m d_m + V_a(h - d_m)\right)dh$$

and it is reduced to

$$F(q(x)) = q(x)h(x) - \frac{V_m d_m{}^2}{\beta+1} - 0.5V_a\left(h^2 - d_m 2\right) - d_m(h - d_m)(V_m - V_a) \tag{14}$$

For a saturated overland flow excess condition ($q(x)$ greater than q_a), $q_a = V_m d_m + V_a(d_a - d_m)$:

$$F(q(x)) = q(x)h(x) - \int_0^{d_m} V_m d_m \left(\frac{h}{d_m}\right)^{\beta} dh - \int_{d_m}^{d_a} (V_m d_m + V_a(h - d_m))dh$$
$$- \int_{d_a}^{h(x)} (V_m d_m + V_a(h - d_m) + \alpha(h - d_m)^m)dh$$

and it is reduced to

$$F(q(x)) = q(x)h(x) - \frac{V_m {d_m}^2}{\beta + 1} - 0.5V_a(h^2 - {d_m}^2) - \frac{\alpha}{m+1}(h - d_a)^{m+1}$$
$$- d_m(h - d_m)(V_m - V_a) \quad (15)$$

By using Equation (13), (14) and(15), the value of *F(q(x))* is calculated and a storage of a slope unit *s* is obtained through Equation(12). The stored water at the entire catchment, S_w, can be calculated by summing the *s* from each slope unit as follows:

$$S_w = \sum_{i=1}^{N} s_i \quad (16)$$

where *N* is the total number of slope units for the entire catchment. Finally, *q* at the catchment outlet is linked to S_w as a function of the effective rainfall intensity and the topographic and physical characteristics of each slope unit, which are derived from DEMs and land use data.

Figure 7 shows study catchments to analyze the change of flow regimes under global warming in the following section. The basins are subdivided into sub-catchments with about 10km^2, and then the lumping method is applied for each sub-catchment; and finally a distributed model composed of lumped sub-catchment models are developed. Figure 8 gives the simulated hydrographs by the full distributed and the distributed-lumped kinematic wave model. The observed discharges and simulated discharges using the full distributed and the distributed-lumped kinematic wave model shows quite good agreements. By applying the lumping method, computational time was reduced to half compared to the simulation using the full distributed model.

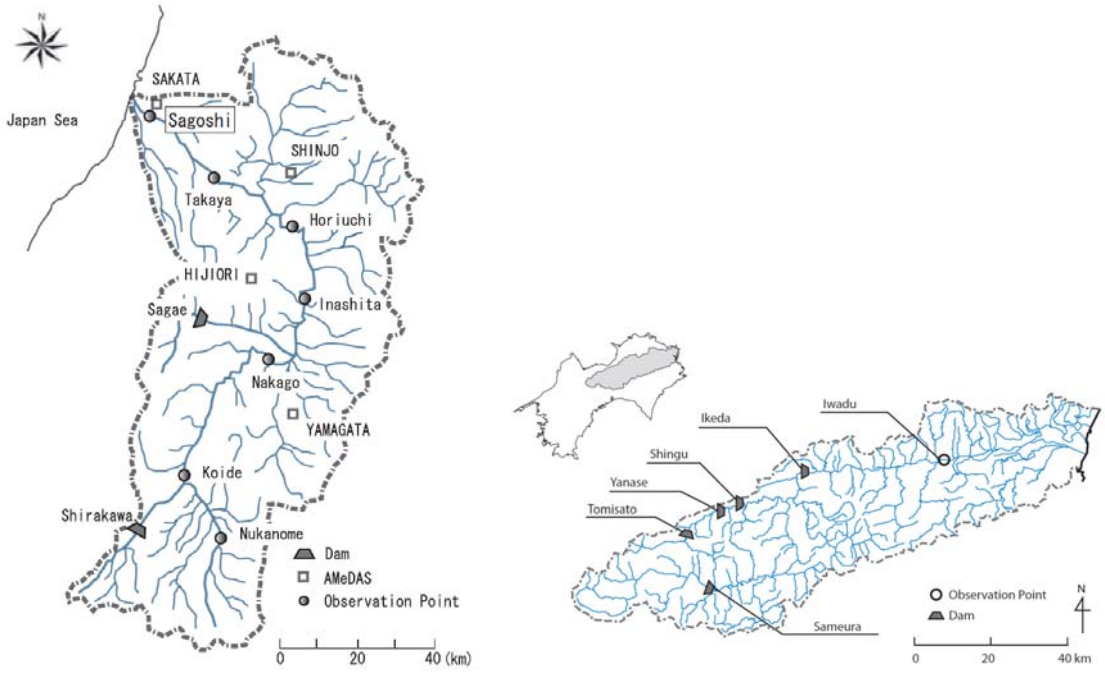

Figure 7. Left: Mogami River basin (7,040km^2). Right: Yoshino River basin (3,750km^2).

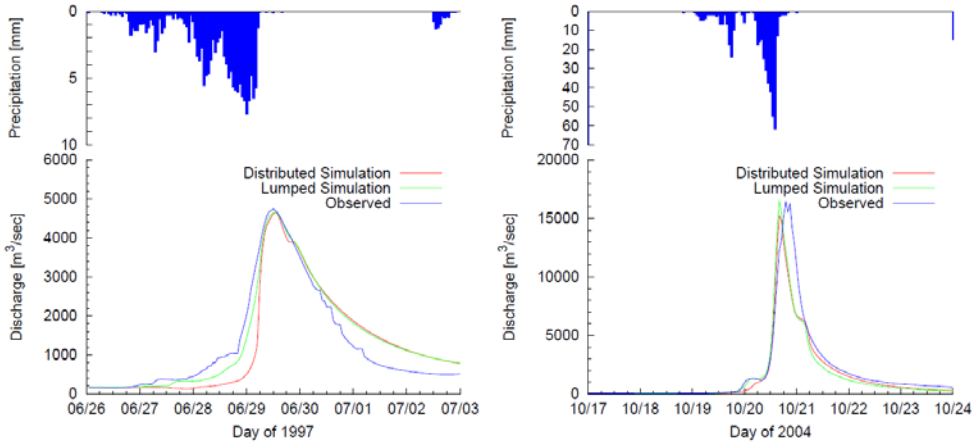

Figure 8. Comparisons of simulated discharges for Mogami River basin (left) and Yoshino River basin (right).

5 STUDY ON THE IMPACT OF CLIMATE CHANGE ON RIVER FLOW REGIME

The impact of climate change on river discharge regime in the Mogami and Yoshino River basins are analyzed by feeding future climate projection data into the lumped-distributed hydrologic model shown above. The projection data consists of hourly precipitation, daily evapotranspiration and daily snow melting of the current climate (1979-2004), the near future climate (2015-2028), and the future climate (2075-2099), which were simulated by a high resolution general circulation model developed by the Meteorological Research Institute, Japan Meteorological Agency.

5.1 Projected hydrologic variables by super-high-resolution atmospheric model

The global atmospheric model (hereafter, AGCM20) performs at a triangular truncation 959 with the linear Gaussian grid (TL959) in the horizontal, which means 1920×960 of grid cells of about 20 km size, and with 60 levels in the vertical (Mizuta *et al*., 2006; Kitoh and Kusunoki, 2007). For the projection simulation, future SST was estimated from the previous AOGCM outputs simulated under the SRES A1B scenario. The AGCM20 output data used for this study are mainly related to hydrologic variables. Five variables as shown in Figure 9 were used as input data for the distributed hydrologic model and it was converted into river discharge data. The PRCSL (rainfall reached to the soil layer, daily) provides effective rainfall amount, and SN2SL (snowmelt into the soil layer, daily) enables the hydrologic model to access the snowmelt amount directly. For more accurate runoff simulations, the daily PRCSL and SN2SL data were downscaled in hourly resolution using the time series of the PRECIPI (rainfall + snowfall, hourly) variables, and the EVPSL (evaporation from the soil layer, daily) and TRNSL (transpiration from the soil root zone, daily) values were used as provided.

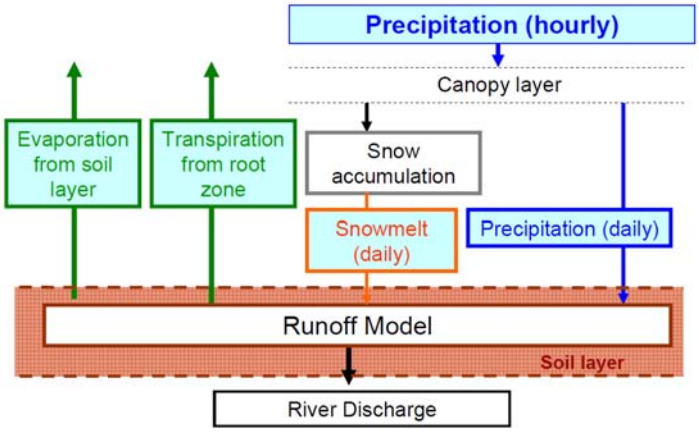

Figure 9. Hydrologic projection data provided by GCM20 used for river discharge simulation.

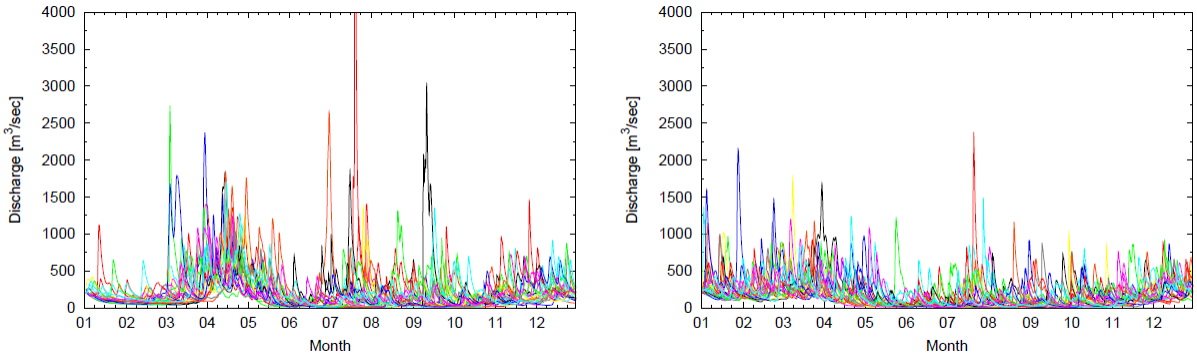

Figure 10. River discharge simulations with GCM20 at Sagoshi (6,500km^2) in the Mogami River basin. Left: Current climate (1979-2004). Right: Future climate (2075-2099).

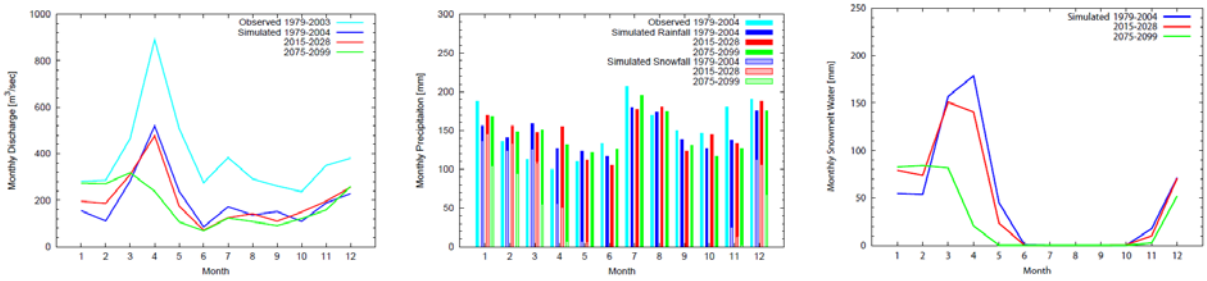

(a) Monthly mean discharge (b) Monthly rainfall and snowfall (c) Monthly snow melting

Figure 11. Change of monthly hydrologic variables at the Mogami River basin.

5.2 Change of river flow regime at the Mogami River basin

Figure 10 shows the simulated river discharge at the Sagoshi station (6,500km^2) in the Mogami River basin using GCM20 projection data for the current climate (1979-2004) and the future climate (2075-2099). It is clearly observed that the peak discharges around April in the current climate disappear in the future climate and the discharges from January to March increase. Figure 11 (a), (b) and (c) shows the monthly mean discharge derived from the hourly runoff simulation, monthly rainfall and snow fall simulated by GCM20, and monthly snow melting simulated by GCM20, respectively.

Figure 11(a) also includes the observed monthly mean discharge during 1979 to 2003. It is found that monthly change of the observed discharge and the simulated discharge is quite well matched though the simulated discharge underestimates observed discharge. The possible reason of the discrepancy is due to overestimation of the discharge observation or underestimation of the observed precipitation. The monthly observed discharge in July is about 170mm in depth; for the same period, the monthly catchment mean precipitation in about 210mm. Evapotranspiration of July is estimated around 100mm. No snowfall in July, thus it is expected that the observed precipitation would be underestimated due to less observatories in the mountainous area. Interesting is the monthly observed precipitation and the simulated precipitation by GCM20 shows quite good agreement in Figure 11(b). This suggests the simulated precipitation would be underestimated than the true precipitation value. Despite the differences, a quite interest finding is the monthly change pattern of observed and simulated river discharge shows a quite good much. This underpins the possible change of the river discharge regimes for the future climate under global warming.

Figure 11(c) shows the change of snowmelting simulated by GCM20. In the future climate, the snowmelting in March, April and May drastically decreases, while it increases in January and February. As a result, the river discharge for the future climate is smoothened. In addition, though monthly precipitation does not change between the current and future climate, the snowfall in winter decreases and rainfall increases. These are the reasons for the drastic change of river discharge. The change pattern could be observed widely in the northern part of Japan. The risk of water resources shortage, especially the risk for agricultural production, and adaptation measures should be analyzed.

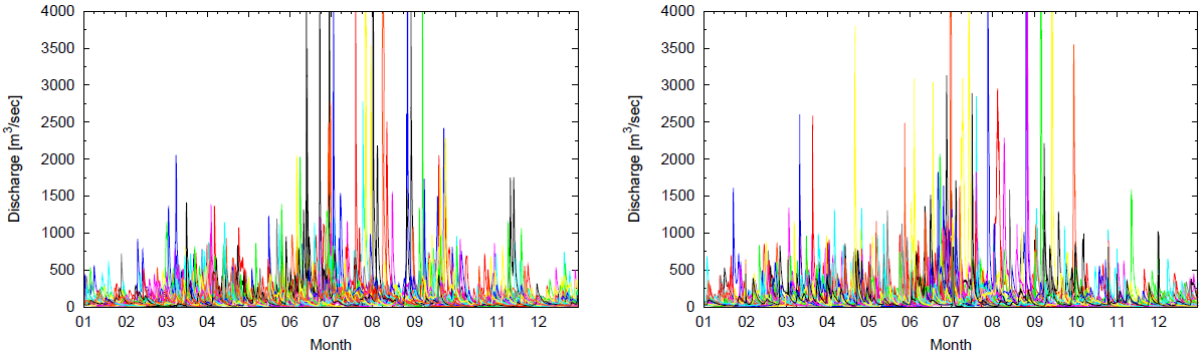

Figure 12. River discharge simulations with GCM20 at Iwazu (2,740km^2) in the Yoshino River basin. Left: Current climate (1979-2004). Right: Future climate (2075-2099).

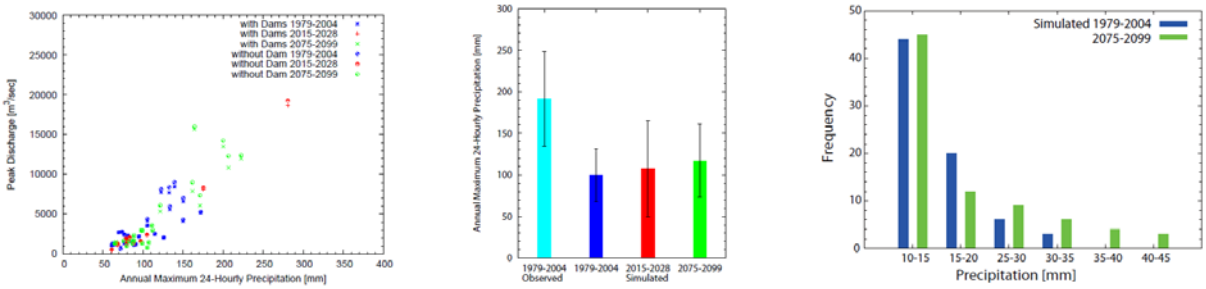

(a) (b) (c)

Figure 13. Change of extreme rainfall characteristics at the Yoshino River basin. (a) Annual maximum catchment mean 24 hours precipitation and peak discharge. (b) Mean and standard variation of the annual maximum 24 hours precipitation. (c) Frequency of one hour precipitation.

5.3 Change of river flow regime at the Yoshino River basin

Figure 12 shows the simulated river discharge at the Iwazu station (2,740km^2) in the Yoshino River basin using GCM20 projection data for the current climate (1979-2004) and the future climate (2075-2099). Based on the discharge simulation, the annual maximum catchment mean 24 hours precipitation and the peak discharges for the corresponding events are plotted in Figure 13(a). It is observed that the annual maximum 24 hours precipitation increases in the future climate compared with the current climate, and the peak discharges becomes higher. Figure 13(b) shows the mean and standard variation of the annual maximum 24 hours precipitation for the periods of the current climate, the near future and the end of 21st century, respectively. The mean values of simulated precipitation by GCM20 are underestimated than observed values, however it is clearly observed the increase tendency of the extreme values. Figure 13(c) shows the frequency of one hour precipitation. It is found that the number of one hour precipitation having more than 20mm clearly increase in the future climate. The simulated precipitation is underestimated than observed values, but the increase tendency of extremes of short term precipitation is suggested. This tendency could be observed widely in the southern part of Japan. The risk of flood and sedimentation disasters and adaptation measures should be analyzed.

6 SUMARRY

A distributed hydrologic model and its lumping procedure are introduced. By using the lumped-distributed hydrologic model, the impact of climate change on river discharge regimes in the Mogami and Yoshino River basins were presented by feeding future climate projection data into the lumped-distributed hydrologic model shown above. The projection data we used consists of hourly precipitation, daily evapotranspiration and daily snow melting of the current climate (1979-2004), the near future climate (2015-2028), and the future climate (2075-2099), which were simulated by a high resolution general circulation model developed by the Meteorological Research Institute, Japan Meteorological Agency.

The findings of the hydrologic simulation are as follows: 1) at the Mogami River basin, floods by snow melting during March to May in the current climate shift to January to March and the flow pattern from January to May would be smoothened in the future climate; 2) at the Yoshino River basin, the magnitude and frequency of severe rainfall would increase and peak flood discharge would increase more highly in the future climate. Further researches include analyzing all Japanese catchments to detect the effect of global warming, to conduct risk analysis of flood and sedimentation disasters and water resources, to develop feasible adaptation measures such as the change of dam operation rule, enhance the hydrologic prediction accuracy.

ACKNOWLEDGEMENTS

The river discharge simulation research is done under the framework of the "Integrated assessment of climate change impacts on watersheds in a disaster environment (PI: Prof. Nakakita, DPRI, Kyoto University)" supported by KAKUSHIN Program of MEXT. Hydrologic projection data used for the river flow simulations was provided by the Meteorological Research Institute, Japan.

REFERENCES

Ichikawa Y and Shiiba M. (2002) Lumping of Kinematic Wave Equation Considering Field Capacity. In *Proceedings of the Third International Conference on Water Resources and Environmental Research.* 22nd-25th of July 2002 at Dresden University of Technology, pp. 56-60.

Innovative Program of Climate Change Projection for the 21st Century (KAKUSHIN Program), MEXT (the Ministry of Education, Culture, Sports Science and Technology, Japan): http://www.kakushin21.jp/jp/index.html (Japanese), http://www.kakushin21.jp/eng/index.html (English).

The Intergovernmental Panel for Climate Change (2007) Climate Change 2007: The Physical Science Basis, Cambridge Univ. Press, Cambridge, UK.

The Intergovernmental Panel for Climate Change (2007) Climate Change 2007: Impacts, Adaptation and Vulnerability, Cambridge Univ. Press, Cambridge, UK.

Kitoh, A. and Kusunoki, S. (2007) East Asian summer monsoon simulation by a 20-km mesh AGCM, Climate Dynamics, DOI 10.1007/s00382-007-0285-2.

Mizuta, R., Oouchi, K., Yoshimura, H., Noda, A., Katayama, K., Yukimoto, S., Hosaka, M., Kusunoki, S., Kawai, H. and Nakagawa, M. (2006) 20-km-mesh global climate simulations using JMA-GSM model -Mean climate states-, *Journal of the Meteorological Soc. of Japan*, **84**, pp. 165–185.

Subcommittee on climate change adaptation for flood control, the River Bureau of the Ministry of Land, Infrastructure, Transport and Tourism, Japan: http://www.mlit.go.jp/river/gaiyou/kikouhendou/index.html (Japanese), http://www.mlit.go.jp/river/gaiyou/kikouhendou/pdf/interimreport.pdf (English).

Sayama, T. and McDonnel, J. J. (2009) A new time-space accounting scheme to predict stream water residence time and hydrograph source components at the watershed scale, *Water Resources Research*, **45**, pp. 1-14.

Tachikawa Y., Nagatani, G. and Takara K. (2004) Development of stage-discharge relationship equation incorporating saturated-unsaturated flow mechanism, *Annual Journal of Hydraulic Engineering, JSCE,* **48**, pp. 7-12.

Tachikawa, Y., Takino, S., Ichikawa, Y. and Shiiba, M. (2009) Study on the impact of climate change on river flow regime in the Mogami and Yoshino river basins. *Annual Journal of Hydraulic Engineering, JSCE,* **53**, pp. 475-480.

Takasao T and Shiiba M. (1988) Incorporation of the effect of concentration of flow into the kinematic wave equations and its application to runoff system lumping, *Journal of Hydrology,* **102**, pp. 301-322.